



OPEN

## Evaluation of $M_xO_y$ /fucoidan hybrid system and their application in lipase immobilization process

Agnieszka Kołodziejczak-Radzimska<sup>1✉</sup>, Michał Bielejewski<sup>2</sup>, Andrzej Biadasz<sup>3</sup> & Teofil Jesionowski<sup>1</sup>

In this work, new  $M_xO_y$ /fucoidan hybrid systems were fabricated and applied in lipase immobilization. Magnesium (MgO) and zirconium (ZrO<sub>2</sub>) oxides were used as  $M_xO_y$  inorganic matrices. In the first step, the proposed oxides were functionalized with fucoidan from *Fucus vesiculosus* (Fuc). The obtained MgO/Fuc and ZrO<sub>2</sub>/Fuc hybrids were characterized by means of spectroscopic analyses, including Fourier transform infrared spectroscopy, X-ray photoelectron spectroscopy, and nuclear magnetic resonance. Additionally, thermogravimetric analysis was performed to determine the thermal stability of the hybrids. Based on the results, the mechanism of interaction between the oxide supports and fucoidan was also determined. Furthermore, the fabricated  $M_xO_y$ /fucoidan hybrid materials were used as supports for the immobilization of lipase from *Aspergillus niger*, and a model reaction (transformation of *p*-nitrophenyl palmitate to *p*-nitrophenol) was performed to determine the catalytic activity of the proposed biocatalytic system. In that reaction, the immobilized lipase exhibited high apparent and specific activity (145.5 U/g<sub>catalyst</sub> and 1.58 U/mg<sub>enzyme</sub> for lipase immobilized on MgO/Fuc; 144.0 U/g<sub>catalyst</sub> and 2.03 U/mg<sub>enzyme</sub> for lipase immobilized on ZrO<sub>2</sub>/Fuc). The immobilization efficiency was also confirmed using spectroscopic analyses (FTIR and XPS) and confocal microscopy.

In recent decades, development of inexpensive, biodegradable, and easily available natural materials in different application have been of more interest for the huge number of researchers. It is highly preferable that the carrier matrix that binds the enzyme can be produced reproducibly and does not disrupt the enzyme activity, because it has a great importance for technological performance and commercial success<sup>1–3</sup>. However, those materials also have some disadvantages (low mechanical strength and limited thermal stability) which can be improved using appropriate modification process<sup>4,5</sup>.

Biopolymers, due to their versatile properties, including non-toxicity, biocompatibility, biodegradability, flexibility, and renewability, are promising carriers for enzyme immobilization<sup>6–8</sup>. In addition, numerous reactive functional groups, such as hydroxyl, amino, or carboxylic acid groups, are present in their chemical structure. These allow enzymes to connect with that structure<sup>7,9</sup>. To date, various natural polysaccharides such as cellulose<sup>10,11</sup>, chitin<sup>12,13</sup>, chitosan<sup>14,15</sup>, alginate<sup>16,17</sup>, agarose<sup>18–20</sup> and carrageenan<sup>21,22</sup> have been used as enzyme supports. Recently, more attention has been paid to biopolymer/inorganic matrix composites or hybrids, which can also be used in enzyme immobilization<sup>7</sup>. High resistance, stability, and availability are the most important parameters of inorganic materials, especially selected oxides (SiO<sub>2</sub>, ZnO, ZrO<sub>2</sub>, MgO, etc.)<sup>23</sup>. Moreover, they can be synthesized via simple and fast methods, which makes them relatively cheap. It should also be noted that biopolymers can be introduced on the surface of metal oxides to increase their affinity to enzymes<sup>7,24</sup>. There is a great deal of information in the literature concerning materials based on chitosan/chitin/cellulose and inorganic oxides, and their application in enzyme immobilization<sup>25–28</sup>.

Natural-derived polysaccharides play an important role in the pharmaceutical and cosmetics industries. They are widely obtained from algae, including brown algae<sup>29,30</sup>. Brown algae (*Phaeophyta*) are a group of algae with a very high degree of specialization in the structure of the thallus, which most often has the form of a branched thread<sup>31–33</sup>. Seaweed is a source of potentially bioactive polysaccharides, among which fucoidan extracted from brown seaweed (especially from *Fucus* species and tissues of echinoderms) is currently the compound

<sup>1</sup>Institute of Chemical Technology and Engineering, Faculty of Chemical Technology, Poznan University of Technology, Berdychowo 4, 60-965 Poznan, Poland. <sup>2</sup>Institute of Molecular Physics Polish Academy of Sciences, M. Smoluchowskiego 17, 60-179 Poznan, Poland. <sup>3</sup>Technical Physics, Faculty of Materials Engineering and Technical Physics, Poznan University of Technology, Piotrowo 3, 60-965 Poznan, Poland. ✉email: agnieszka.kolodziejczak-radzimska@put.poznan.pl

being studied most extensively<sup>34,35</sup>. Fucoidan can be obtained from a number of marine sources, including sea cucumbers<sup>36</sup> and brown algae<sup>37</sup>. A high fucoidan content has been established in a large number of algae and invertebrates, for example, *Fucus vesiculosus*, *Sargassum stenophyllum*, *Chorda filum*, *Ascophyllum nodosum*, *Dictyota menstrualis*, *Fucus evanescens*, *Fucus serratus*, *Fucus distichus*, *Caulerpa racemosa*, *Hizikia fusiforme*, *Padina gymnospora*, *Kjellmaniella crassifolia*, *Analipus japonicus*, and *Laminaria hyperborea*. Different types of fucoidan are present in these sources, and various extraction methods are used to obtain them<sup>38</sup>.

Fucoidan consists of  $\alpha$ -L-fucopyranose molecules, which may be connected by 1→3 bonds or by alternating 1→3 and 1→4 bonds. To obtain the branched structure in the main chain, radicals of  $\alpha$ -L-fucopyranose are attached, as well as inorganic sulfate(VI) radicals and radicals of organic such as D-glucuronic and acetyl. Several of the fucoidan structures have also contain small amounts of various other monosaccharides e.g. glucose, galactose, xylose, and/or mannose<sup>39–42</sup>. Fucoidan offers a variety of biological properties, including antibacterial, antioxidant, antiviral, anti-inflammatory, anticoagulant, and anticancer properties<sup>43–45</sup>. In addition, fucoidan is biocompatible, biodegradable, and nontoxic<sup>46,47</sup>.

Due to its unique features, fucoidan is a promising biopolymer that can also be utilized as a coating material. To date, fucoidan-modified materials have been used in medical applications such as drug delivery<sup>48–52</sup>. The magnetic mesoporous silica system was modified with fucoidan by Moorthy et al.<sup>48</sup>. Fucoidan was applied to the silica surface by a metal–ligand complex coordination technique. The proposed material was utilized as a drug carrier and as a hyperthermia agent for chemotherapy and magnetic hyperthermia-based thermal therapy applications in emerging cancer therapy. In other studies, fucoidan was coated on CuS nanoparticles and applied in chemophotothermal therapy against cancer cells<sup>49</sup>. In this case, fucoidan was introduced onto the CuS surface by a layer-by-layer technique using polycationic and anionic compounds. In another study, Shin et al.<sup>50</sup> developed fucoidan-coated manganese dioxide nanoparticles (Fuco-MnO<sub>2</sub>-NPs) and tested them in the clinical treatment of cancer. The MnO<sub>2</sub>-NPs were coated with fucoidan by the adsorption method. Venkatesan et al.<sup>51</sup> used a fucoidan–chitosan complex to modify silver nanoparticles (AgNP). This system has high potential for food and cosmetic applications. Another research team designed bimodal fucoidan-coated zinc oxide/iron oxide nanoparticles for medical applications<sup>52</sup>.

Until now, inorganic materials modified with fucoidan have not been investigated as supports for enzyme immobilization. Therefore, in this study, selected inorganic M<sub>x</sub>O<sub>y</sub> compounds (ZrO<sub>2</sub> and MgO) were modified with fucoidan (Fuc). A key objective was to confirm the modification of M<sub>x</sub>O<sub>y</sub> with fucoidan using a range of spectroscopic analyses—Fourier transform infrared spectroscopy (FTIR), nuclear magnetic resonance spectroscopy (NMR), and X-ray photoelectron spectroscopy (XPS). Additionally, thermogravimetric analysis (TG/DTG) was performed. The prepared M<sub>x</sub>O<sub>y</sub>/Fuc materials were then used as supports for lipase. The amount of immobilized lipase, catalytic activity, and confocal microscopic images were analyzed to confirm the success of the immobilization.

## Experimental part

**Materials.** The following materials were used in the study: zirconium isopropoxide (TPZ), 25% ammonia solution (NH<sub>3(aq)</sub>), ethyl alcohol (EtOH), magnesium oxide powder, fucoidan from *Fucus vesiculosus* (Fuc), lipase from *Aspergillus niger* (LAN), sodium phosphate (NaH<sub>2</sub>PO<sub>4</sub>), dibasic sodium phosphate (Na<sub>2</sub>HPO<sub>4</sub>), *p*-nitrophenyl palmitate (*p*-NPP), *p*-nitrophenol (*p*-NP), 2-propanol, Triton X-100 and Arabic gum. All of these materials were purchased from Sigma-Aldrich (Saint Louis, MO, USA).

**M<sub>x</sub>O<sub>y</sub>/Fuc hybrid preparation.** The high-purity magnesium oxide powder (98%) used in these studies was purchased from Sigma-Aldrich. ZrO<sub>2</sub> was synthesized using the sol–gel method. In this case, zirconium isopropoxide and ammonium were dosed into a reactor containing ethanol. The mixture was stirred for 1 h. The next step of the synthesis was crystallization (ageing; 24 h). The resulting zirconium oxide (ZrO<sub>2</sub>) was washed with water and filtered, and then dried at 105 °C.

At the next stage of the research, ZrO<sub>2</sub> and MgO were modified with fucoidan. For this purpose the water solution of fucoidan (1 mg/mL) was prepared, 1 g of the appropriate oxide was added to the fucoidan solution (10 mL), and it was stirred magnetically for 24 h. The resulting M<sub>x</sub>O<sub>y</sub>/Fuc hybrid system was filtered and dried at 60 °C. The samples obtained were labeled ZrO<sub>2</sub>/Fuc and MgO/Fuc.

**Spectroscopic analysis.** To confirm both the functionalization of ZrO<sub>2</sub> and MgO with fucoidan and the immobilization process, spectroscopic analyses were performed: Fourier transform infrared spectroscopy (FTIR), nuclear magnetic resonance (<sup>1</sup>H and <sup>13</sup>C NMR) and X-ray photoelectron spectroscopy (XPS). A detailed description of these analyses is given in the Supplementary Materials.

**Thermogravimetric analysis.** Thermogravimetric analysis (TG/DTG) was performed using a Jupiter STA 449F3 thermogravimetric analyzer (Netzsch, Germany). Measurements were carried out under flowing nitrogen at a heating rate of 5 °C/min and in a temperature range of 30 to 1000 °C, with an initial sample weight of approximately 5 mg.

**Enzyme immobilization.** ZrO<sub>2</sub>/Fuc and MgO/Fuc were used as supports for lipase immobilization. The process was performed by an adsorption method. A specified amount of matrix was shaken with the lipase solution (5 mg/mL, phosphate buffer at pH = 7) in an incubator (20 °C, IKA-Werke, Staufen, Germany) for 24 h. Then the prepared biocatalytic system (ZrO<sub>2</sub>/Fuc/LAN or MgO/Fuc/LAN) was separated by filtration. Bradford analysis<sup>53</sup> was used to confirm the result of the immobilization process and to calculate the amount of immobilized lipase ( $P_{LAN}$ , mg<sub>enzyme</sub>/g<sub>support</sub>) and the immobilization performance (PI, %). In the next step, the

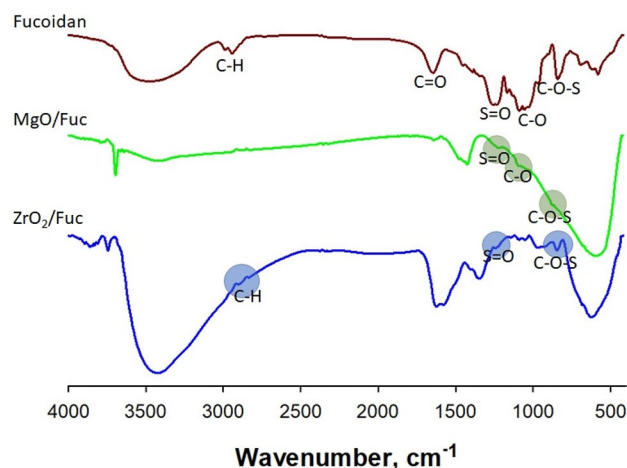


**Figure 1.** FTIR spectra of fucoïdan, MgO/Fuc, and ZrO<sub>2</sub>/Fuc.

enzymatic activity of the immobilized lipase was evaluated. The model reaction used was the transformation of *p*-NPP (*p*-nitrophenyl palmitate) to *p*-NP (*p*-nitrophenol). The release of the product was observed at 410 nm (using a JASCO V650 spectrophotometer, Japan). All reactions (performed in triplicate) were carried out with stirring at 1000 rpm for 2 min at 30 °C. Based on the results, the apparent ( $U/g_{\text{catalyst}}$ ), specific ( $U/mg_{\text{enzyme}}$ ), and relative (%) activities were estimated. The equations used to calculate activity are given in the Supplementary Materials. Kinetic parameters, including the Michaelis–Menten constant ( $K_M$ ) and maximum reaction velocity ( $V_{\text{max}}$ ) were determined by means of an enzymatic assay based on the same reaction mentioned above, using various concentrations of the substrate solution (0.005–1.5 M). The apparent kinetic parameters of the free and immobilized enzyme were calculated based on the Hanes–Woolf plot. The immobilization efficiency was also indirectly confirmed by FTIR and XPS analysis.

**Confocal microscopy.** The morphology of the  $M_xO_y$ /Fuc hybrids and immobilized lipase was evaluated on the basis of confocal laser scanning microscopy (CLSM) photographs (LSM710, Zeiss, Germany), obtained using an argon laser (488 nm). In material mode (reflected light), the laser operated at a wavelength of 458 nm. In fluorescence mode, the laser operated at 488 nm and fluorescence was observed in the range 510–797 nm.

## Results and discussion

**Spectroscopic analysis of ZrO<sub>2</sub>/Fuc and MgO/Fuc hybrids.** Spectroscopic analysis is employed to explore hybrid materials, providing practical information such as elemental type, chemical composition, optical and electronic properties, and crystallinity. In this study, spectroscopic analyses were used to confirm the functionalization of ZrO<sub>2</sub> and MgO with fucoïdan. The characteristic groups in the fucoïdan structure were precisely interpreted based on the FTIR spectrum (Fig. 1). The following bands were identified: OH group of monosaccharide monomer (at 3500 cm<sup>-1</sup>); aliphatic C–H (at 2983 and 2945 cm<sup>-1</sup>); O–C–O stretching vibrations (at 1635 cm<sup>-1</sup>); asymmetric stretching vibrations of S=O in the sulfate group (at 1258 cm<sup>-1</sup>); ether bond C–O (at 1070 cm<sup>-1</sup>); C–O–S (at 846 cm<sup>-1</sup>); and a characteristic band for deoxy sugars such as fucose (at 572 cm<sup>-1</sup>). Additionally, a signal at 846 cm<sup>-1</sup> corresponds to sulfation in the equatorial position, where the sulfate ester binds to the C-2 of fucose to form sulfate fucose<sup>54,55</sup>.

The FTIR spectra of MgO and ZrO<sub>2</sub> modified with fucoïdan are presented in Fig. 1. They confirm that the metal oxide was successfully functionalized with fucoïdan. The characteristic groups of pure oxide (Fig. 1S) and fucoïdan appear on the FTIR spectra of MgO/Fuc and ZrO<sub>2</sub>/Fuc. On the FTIR spectrum of MgO/Fuc (Fig. 1) the following fucoïdan groups are present: OH (at 3450 cm<sup>-1</sup>); C=O (at 1650 cm<sup>-1</sup>); S=O (at 1450 cm<sup>-1</sup>); C–O (at 1150 cm<sup>-1</sup>). The small band for C–O groups and the small and broad band for OH groups indicate the direct connection of the fucoïdan with the MgO surface.

The FTIR spectrum for ZrO<sub>2</sub>/Fuc contains bands for OH (at 3450 cm<sup>-1</sup>); C–H (at 2900 cm<sup>-1</sup>); S=O (1400 cm<sup>-1</sup>); and C–O–S (at 800 cm<sup>-1</sup>) (Fig. 1). The broad and intensive band with a maximum at 3500 cm<sup>-1</sup> indicates the connection of fucoïdan with ZrO<sub>2</sub> via hydrogen bonds of water molecules. This is further evidenced by the shift in this band relative to the band obtained for pure fucoïdan. The narrow and weak peak at 3700 cm<sup>-1</sup> may originate from pure water, which may attach to the fucoïdan-modified surface of ZrO<sub>2</sub> during the fucoïdan functionalization process in aqueous solution.

XPS spectroscopy was also used to confirm the functionalization of MgO and ZrO<sub>2</sub> with fucoïdan. The results are shown in Fig. 2. On the surface of MgO and ZrO<sub>2</sub> (Fig. 2S), elements such as magnesium, zirconium, and oxygen are present. The MgO/Fuc and ZrO<sub>2</sub>/Fuc hybrids contain the same elements, but carbon and sulfur are also present, which is a consequence of the modification with fucoïdan (Fig. 2a).

Additional information on the interaction of fucoïdan with the surface of the inorganic oxide is provided by a detailed analysis of the C 1s and S 2p lines of the XPS spectrum. The XPS C 1s and S 2p lines of the MgO/Fuc and ZrO<sub>2</sub>/Fuc hybrids are shown in Fig. 2b. Carbon and sulfur atoms are not present on the surface of MgO

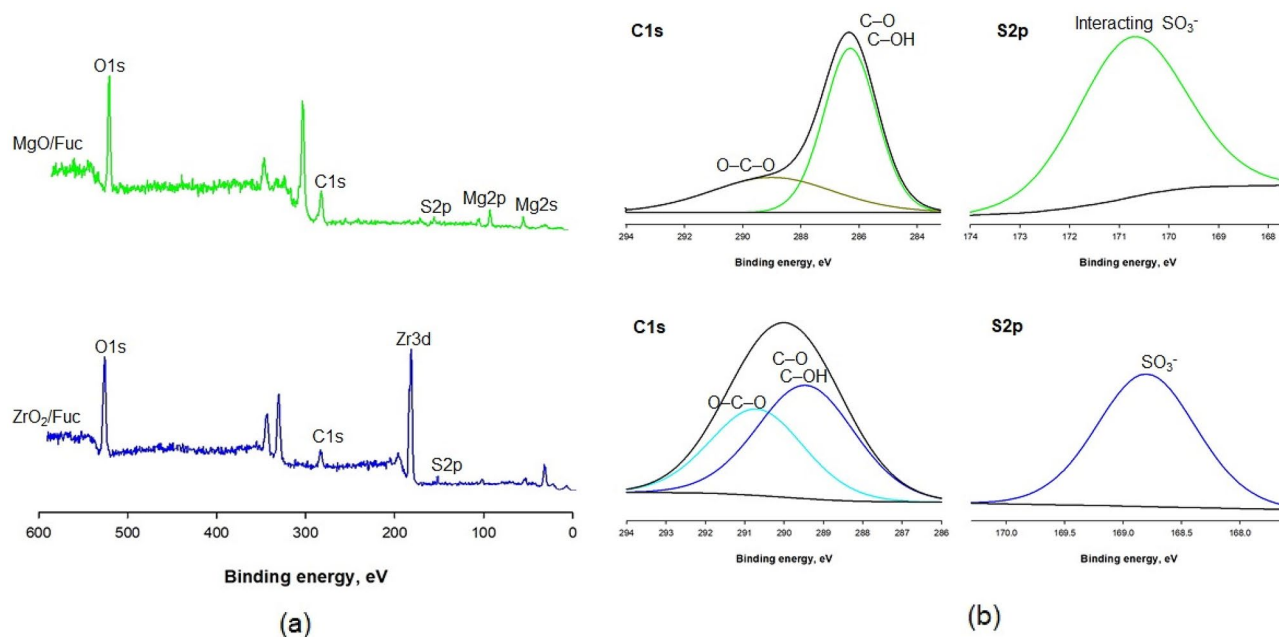


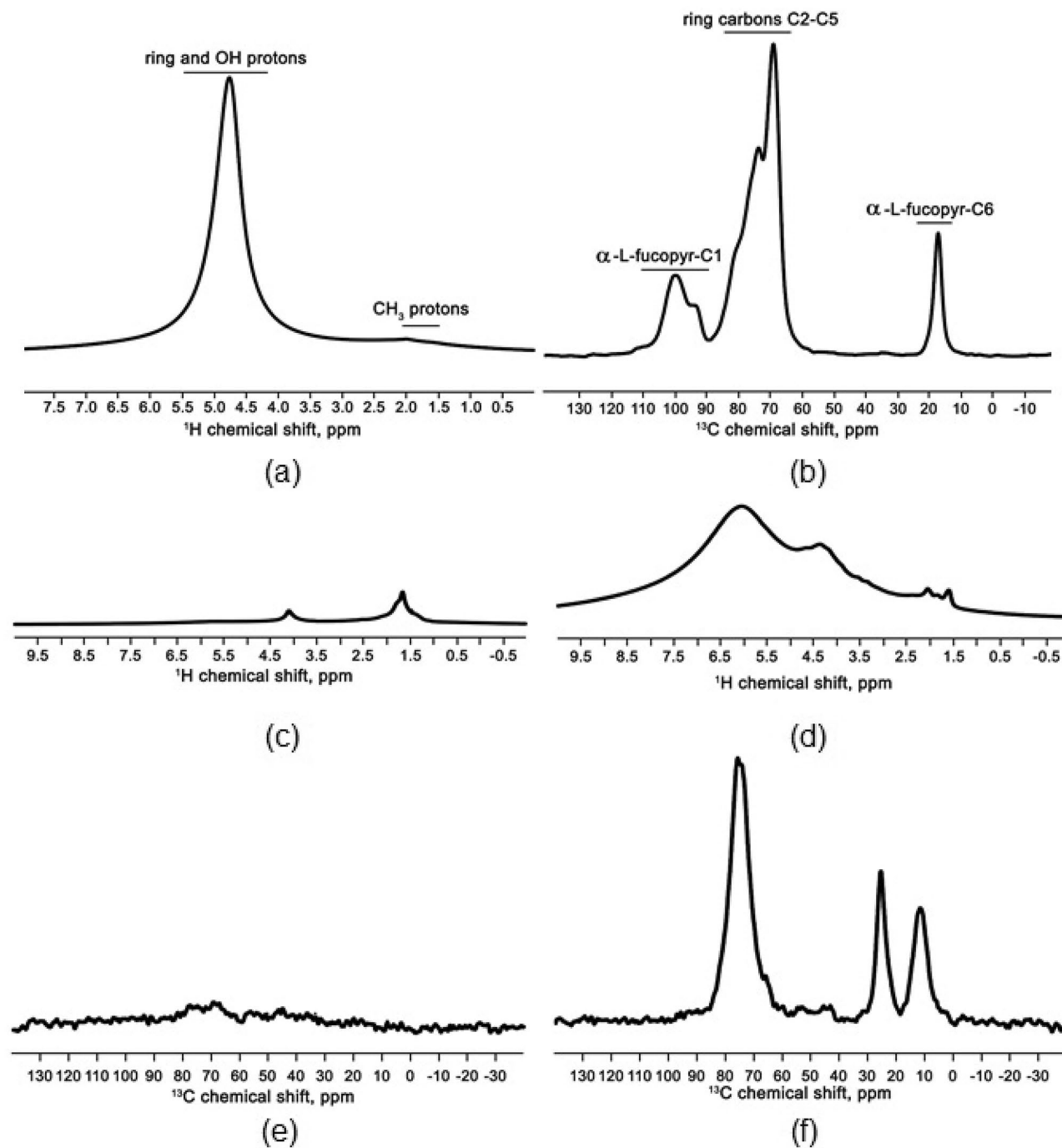
**Figure 2.** XPS survey spectra of MgO/Fuc and ZrO<sub>2</sub>/Fuc (a), and the deconvoluted XPS of C 1s for MgO/Fuc; S 2p for MgO/Fuc; C 1s for ZrO<sub>2</sub>/Fuc; and S 2p for ZrO<sub>2</sub>/Fuc (b).

and ZrO<sub>2</sub> (Fig. 2S). In the XPS C 1s line for MgO/Fuc, the two C 1s peaks were identified at around 288.7 eV and 286.2 eV, corresponding respectively to O–C–O and C–OH/C–O bonds. Here, the C–OH/C–O bonds are more expanded. A different situation is observed with the C 1s line for ZrO<sub>2</sub>/Fuc. In this case, the two C 1s peaks are also recognized at around 290.8 eV (O–C–O) and 289.4 eV (C–OH/C–O). However, the size of these peaks is similar. Deconvolution of the fucoidan S 2p spectral peak shows two sulfur chemical environments at approximately 167.0 eV (for the –SO<sub>3</sub><sup>–</sup> group) and 170.9 eV (for the interacting –OSO<sub>3</sub><sup>–</sup> group)<sup>56–58</sup>. For MgO/Fuc and ZrO<sub>2</sub>/Fuc, only one sulfur environment was observed, at binding energies of 170.7 eV (interacting –OSO<sub>3</sub><sup>–</sup> group) and 168.8 eV (–SO<sub>3</sub><sup>–</sup> group) respectively (Fig. 2b). The change in the binding energy peak may indicate interactions of some fucoidan sulfate groups with the surface of the metal oxide<sup>58</sup>.

The <sup>1</sup>H and <sup>13</sup>C spectra of pure fucoidan (Fig. 3) provide us with information about the structure of the pure polysaccharide and the characteristic hydrogen bond pattern of the material used, and serve as a reference for the analysis of the data obtained for the investigated samples. Moreover, since the samples were obtained by wet synthesis, a signal from residual water molecules was expected to be found in the <sup>1</sup>H spectra of the functionalized matrices. <sup>13</sup>C spectra were used to confirm that fucoidan molecules were present in the matrices. Differences in <sup>13</sup>C spectra between the neat fucoidan sample and the functionalized one will indicate a change in the structure of the polysaccharide chain caused by interaction with the surface of the matrix. As fucoidan molecules can form hydrogen bonds, the change in the <sup>1</sup>H spectra would indicate a mechanism of functionalization of the surface of the matrices with fucoidan molecules, based on the creation of hydrogen bonds between the surface of the matrix and the fucoidan molecules.

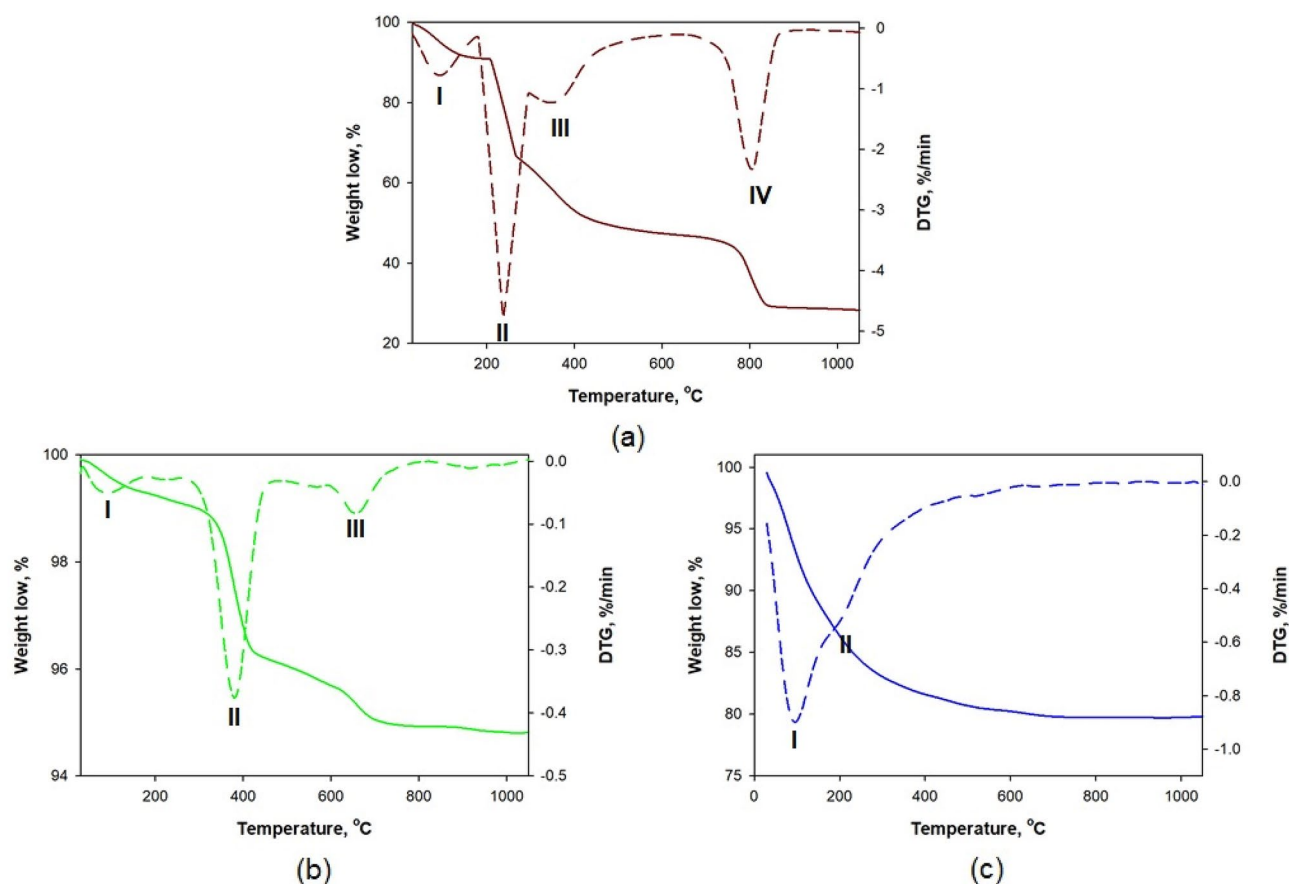
The <sup>1</sup>H spectrum (Fig. 3a) shows an intense signal in the region 5.5–4.25 ppm, which comes from ring protons bonded to C2–C5 carbons, OH groups of fucoidan and residual water molecules. Small signals at 2–1.5 ppm originate from methyl groups located at C6 carbons. The <sup>13</sup>C spectrum (Fig. 3b) shows a strong signal at 16.8 ppm identified as C6 carbons in methyl groups, while the broad signal at 85–60 ppm comes from C2–C5 ring carbons, and the signal at 100 ppm from C1 carbons.

Figure 3c–f shows the <sup>1</sup>H and <sup>13</sup>C spectra recorded for matrices functionalized with fucoidan molecules. In the ZrO<sub>2</sub>/Fuc <sup>1</sup>H spectrum a strong OH signal from fucoidan and residual water is observed (Fig. 3c). The observed change in the chemical shift of the most intense signal in the range 5.5–4.25 ppm is related to the OH groups in fucoidan and residual water, indicating that the structure of the hydrogen bonds present in the samples is changed. In the case of ZrO<sub>2</sub> (Fig. 3c), a splitting of the signal in a range from 7.5 to 3.5 ppm can be observed. This splitting is caused by OH groups involved in the creation of hydrogen bonds between fucoidan molecules and the surface of the ZrO<sub>2</sub> matrix. The peak shifts towards lower fields by 1.4 ppm, indicating the creation of strong hydrogen bonds. The second peak appearing at 4.3 ppm corresponds very well to proton signals from the ring unit of the fucoidan molecule. Together with the lack of change in the signal position at 2–1.5 ppm, this implies that the mechanisms of functionalization of the ZrO<sub>2</sub> matrix with fucoidan are due to the creation of hydrogen bonds. The MgO matrix used was purchased commercially and used without further preparation for the functionalization procedure. The proton spectra of this matrix functionalized with fucoidan are shown in Fig. 3e. Only small signals from fucoidan molecules were detected, with no peak from residual water molecules. The observed chemical shifts correspond to those of fucoidan molecules found in the literature, and no shift of the hydroxyl group signal was detected.



**Figure 3.** Solid-state DP/MAS SE  $^1\text{H}$  NMR spectrum (a) and CP/MAS  $^{13}\text{C}$  NMR spectrum (b) of fucoidan at room temperature. Solid-state DP/MAS  $^1\text{H}$  NMR spectra for MgO/Fuc (c) and ZrO<sub>2</sub>/Fuc (d) at room temperature; and solid-state CP/MAS  $^{13}\text{C}$  NMR spectra for MgO/Fuc (e) and ZrO<sub>2</sub>/Fuc (f) at room temperature.

Direct evidence of the presence of fucoidan molecules in the studied matrices is provided by the  $^{13}\text{C}$  spectra. The  $^{13}\text{C}$  spectra of the studied samples are shown in Fig. 3e,f. Only the ZrO<sub>2</sub> matrix functionalized with fucoidan shows well-detectable signals from the fucoidan units; in the case of MgO matrices only very weak signals from aromatic carbons were detected. By comparing the  $^1\text{H}$  and  $^{13}\text{C}$  spectra of the studied samples we can draw conclusions about the chemical composition of the samples. The MgO matrix purchased commercially was found to be free of any impurities after the synthesis processes, but only a very small amount of fucoidan molecules was found in the functionalized matrix. The weak  $^1\text{H}$  signals from the fucoidan molecules indicate a very low quantity of this substance, which is also confirmed by the almost undetectable  $^{13}\text{C}$  signals from the fucose unit. Another important finding is that the signals from residual water molecules expected to be left after the functionalization process are also missing.



**Figure 4.** TG/DTG curves of fucoidan (a); MgO/Fuc (b); and ZrO<sub>2</sub>/Fuc (c).

On the basis of the spectroscopic analyses it can be concluded that the functionalization of oxide materials with fucoidan molecules was successful. However, the NMR analysis shows that a better effect was achieved for ZrO<sub>2</sub>. Fucoidan molecules were shown to attach to the surface of the ZrO<sub>2</sub> matrix by way of hydrogen bonds; the molecules may be attached directly or via residual water molecules. Furthermore, only a very small trace of fucoidan units was found after functionalization of MgO. Also, it is important to note that no signal from the hydroxyl groups of water molecules was detected in this sample. Therefore, it can be concluded that water plays an important role in the functionalization procedure and mediates the binding of fucoidan molecules to the surface of the matrix. In addition, FTIR and XPS analyzes confirm the positive modification with fucoidan, where the characteristic bonds/picks for fucoidan are observed.

**Thermogravimetric analysis of MgO/Fuc and ZrO<sub>2</sub>/Fuc.** Figure 4 shows the TG/DTG curves of fucoidan and the MgO/Fuc and ZrO<sub>2</sub>/Fuc hybrids. The fucoidan thermogram (Fig. 4a) presents four mass loss steps. The first mass loss (exothermic peak I) of 6% at 100 °C corresponds to physically adsorbed water. The second and third, at 240 °C (approximately 22%, exothermic peak II) and 355 °C (42%, exothermic peak III) are associated with the loss of sulfate groups. The final mass loss, of approx. 70%, occurring at 800 °C (exothermic peak IV) is probably related to the decomposition of carbon residues<sup>48,59</sup>. Furthermore, changes are observed between the TG/DTG curves of pure inorganic oxide (Fig. 6S) and the sample after fucoidan functionalization (Fig. 4b,c). The MgO/Fuc sample exhibited a total mass loss of 5%. The mass loss took place in three steps, with major losses in the second stage (ca. 4% at 380 °C) and in the third (5% at 650 °C), probably corresponding to the collective decomposition of the surface-coating fucoidan polymeric units<sup>59</sup>. A change in total mass loss is also observed on the TG/DTG curves of ZrO<sub>2</sub> (Fig. 8S) and ZrO<sub>2</sub>/Fuc (Fig. 4c). In this case, the ZrO<sub>2</sub>/Fuc hybrid loses about 20% of its total mass. Here, only two exothermic peaks are observed (at 100 and 220 °C), associated with physically and chemically adsorbed water. The nature of the mass loss and the missing peak above 600 °C suggest that the fucoidan molecules evaporated from the system before the decomposition of carbon residues occurred. This can be understood if the fucoidan molecules were bonded to the ZrO<sub>2</sub> surface via water molecules.

However, the changes in the total mass loss of both samples after fucoidan modification (MgO/Fuc and ZrO<sub>2</sub>/Fuc) suggest that fucoidan was successfully incorporated on the surface of MgO and ZrO<sub>2</sub>.

**Enzyme immobilization.** The designed MgO/Fuc and ZrO<sub>2</sub>/Fuc hybrid materials were used as supports for lipase immobilization. The effect of pH on lipase immobilization was investigated as shown in Fig. 5. The

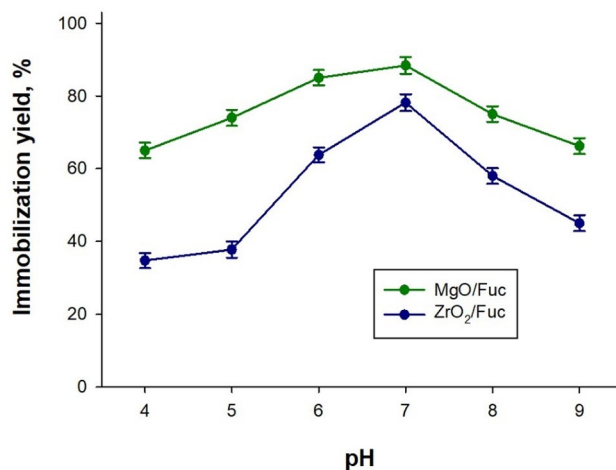


**Figure 5.** Effect of pH on the immobilization of lipase from *Aspergillus niger* on MgO/Fuc and ZrO<sub>2</sub>/Fuc.

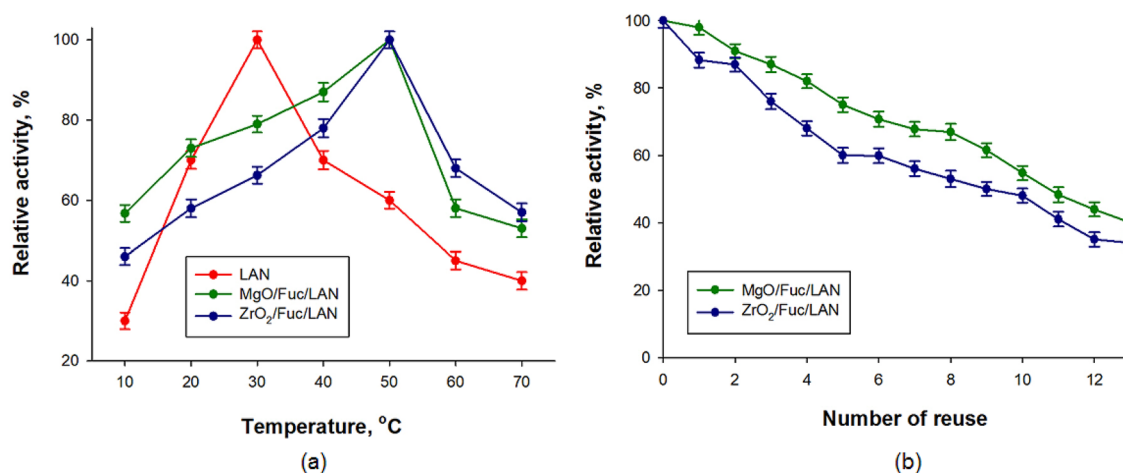


**Figure 6.** Influence of temperature (a) and repeated use on the catalytic activity of free and immobilized lipase (b).

immobilization yield lipase on MgO/Fuc increased from 65% at pH 4 to the highest value of 88.4% at pH 7.0, but decreased to 66.2% at pH 9. The immobilization yield of lipase on ZrO<sub>2</sub>/Fuc showed a similar tendency, which was 34.8% at pH 4, reaching the highest value of 78.2% at pH 8, and decreased to 45% at pH 9. The protons bind to the lone pair electrons on the amino N atom under acidic conditions. Whereas under pH 8, the hydrogen bonds on support will be broken in alkalinity conditions<sup>4,5</sup>. Based on the information, the optimal pH for immobilization was determined to be 7.0.

Basic information on enzyme immobilization efficiency and the catalytic activity of lipase immobilized on MgO/Fuc and ZrO<sub>2</sub>/Fuc is given in Table 1S. The results for catalytic parameters indicate that the materials proposed in this study (both MgO/Fuc and ZrO<sub>2</sub>/Fuc) can be used as supports for the enzyme. The amount of lipase immobilized was 91.8 mg on 1 g of MgO/Fuc, and 70.8 mg on 1 g of ZrO<sub>2</sub>/Fuc. The immobilization efficiencies were 61.2% and 78.6%, respectively. The obtained biocatalytic systems (MgO/Fuc/LAN and ZrO<sub>2</sub>/Fuc/LAN) exhibited similar catalytic activities. Lipase immobilized on MgO/Fuc had apparent and specific activities of 145.5 U/g<sub>catalyst</sub> and 1.58 U/mg<sub>enzyme</sub>, while the corresponding values for the ZrO<sub>2</sub>/Fuc/LAN biocatalytic system were  $A_{Ap} = 144.0$  U/g<sub>catalyst</sub> and  $A_S = 2.03$  U/mg<sub>enzyme</sub>.

The influence of temperature and reuse over several cycles on the enzymatic activity of the immobilized lipase was evaluated (Fig. 6). The results show that lipase immobilized on both MgO/Fuc and ZrO<sub>2</sub>/Fuc retained above 40% of its activity at temperatures in the range 20 to 70 °C (Fig. 6a). In both cases (MgO/Fuc/LAN and ZrO<sub>2</sub>/Fuc/LAN) the maximum activity was achieved at 50 °C, which indicates that lipase immobilized on the proposed materials can be used in harsher conditions. Moreover, the immobilized enzyme has a heterogeneous form and can be used over several enzymatic reaction cycles. The tests showed that the proposed biocatalytic systems (MgO/Fuc/LAN and ZrO<sub>2</sub>/Fuc/LAN) retained ca. 40% of their initial activity after 12 cycles (Fig. 6b).

In addition the kinetic parameters like Michaelis–Menten constant ( $K_M$ ) and maximum reaction velocity ( $V_{max}$ ) were determined. The obtained results are shown in Table 1. A lower  $K_M$  value after immobilization

Sample	$K_M$ , mM	$V_{max}$ , mM/min
Free lipase from <i>Aspergillus niger</i>	$0.58 \pm 0.02$	$43.55 \pm 0.6$
Lipase immobilized on MgO/Fuc	$0.68 \pm 0.02$	$51.74 \pm 0.7$
Lipase immobilized on ZrO <sub>2</sub> /Fuc	$0.61 \pm 0.03$	$49.53 \pm 0.7$

**Table 1.** Kinetic parameters ( $K_M$  and  $V_{max}$ ) of free and immobilized lipase from *Aspergillus niger*.

Support	Lipase origin	Amount of immobilized lipase (mg/g)	Enzymatic activity (U/g)	Reusability	Ref.
Chitin/graphene oxide	<i>Candida rugosa</i>	141.4	–	30% after 5 cycles	<sup>60</sup>
Chitosan/mesoporous silica	<i>Porcine pancreas</i>	132.1	328.0	90% after 9 cycles	<sup>61</sup>
Magnetic nanoparticles coated with chitosan	<i>Aspergillus niger</i>	3.86	238.5	80% after 14 cycles	<sup>62</sup>
Cellulose/Fe <sub>2</sub> O <sub>3</sub>	<i>Rhizomucor miehei</i>	700	125.5	50% after 10 cycles	<sup>63</sup>
MgO/fucoidan	<i>Aspergillus niger</i>	91.8	145.5	50% after 12 cycles	This study
ZrO <sub>2</sub> /fucoidan	<i>Aspergillus niger</i>	80.7	144.1	40% after 12 cycles	This study

**Table 2.** Comparison of the present results with literature data on lipase immobilization on various polysaccharide-based hybrids.

indicates a higher binding ability with respect to the substrate. While, the higher  $V_{max}$  suggesting that the immobilized lipase can catalyze the reaction faster than free lipase.

Chitin, chitosan, and cellulose are the polysaccharides most commonly used to modify inorganic oxides. A comparison of the results obtained in this study with previous results on lipase immobilization on various polysaccharide-based hybrids is shown in Table 2. The results show that materials based on polysaccharide and inorganic oxide can be successfully applied as supports for the immobilization of lipase (of various origins). Different types of lipase (from *Candida rugosa*, *Porcine pancreas*, *Aspergillus niger* and *Rhizomucor miehei*) were immobilized on the following matrices: chitin/graphene oxide, chitosan/mesoporous silica, magnetic nanoparticles coated with chitosan, and cellulose/Fe<sub>2</sub>O<sub>3</sub><sup>60–63</sup>. The immobilized lipases exhibited enzymatic activity in the range 125–328 U/g, and could be used over several reaction cycles (from 5 to 14), retaining 50–90% of their initial activity. The results obtained in the present study are similar to others; the observed difference is probably due to the use of different kinds of lipases, which exhibit different enzymatic activities in their native form.

The success of the immobilization process was also indirectly confirmed by the results of FTIR and XPS analysis, which are presented as spectra in Fig. 6.

Based on the FTIR spectra (Fig. 7a), it is concluded that most of the characteristic groups for lipase are also observed on the surface of the proposed biocatalytic system. The following main signals are present in the FTIR spectrum of lipase: stretching vibrations of N–H bonds at 3220 cm<sup>-1</sup>, amide I, II, and III bands (from 1650 to 1410 cm<sup>-1</sup>), and stretching of C–O bonds at 1080 cm<sup>-1</sup>. The changes observed between the FTIR spectra of the pure support (Fig. 1) and the system with immobilized lipase confirm the success of the immobilization process. On the FTIR spectrum of MgO/Fuc/LAN, the greatest changes are observed in the amide III and –C–O bands, while the ZrO<sub>2</sub>/Fuc/LAN spectrum exhibits changes in the N–H and C–O bands.

The XPS spectrum of free lipase (Fig. 7b) contains three characteristic peaks at binding energies of 531.0 eV, 400.7 eV and 287.7 eV, which are related to O 1s, N 1s and C 1s. The same peaks are observed in the survey spectra of MgO/Fuc/LAN and ZrO<sub>2</sub>/Fuc/LAN, confirming the presence of lipase on the hybrid material's surface. Most important is the presence of N 1s peaks (Fig. 7c; not observed on the pure support—see Fig. 2), which can be attributed to the CO–NH– and amino groups of lipase, and provide further evidence of the immobilization of lipase on the oxide functionalized with fucoidan<sup>59</sup>. Furthermore, changes in the C 1s deconvolution lines also confirm lipase immobilization (see Fig. 5S).

In addition, it was found that MgO/Fuc and ZrO<sub>2</sub>/Fuc exhibited increased intensity of fluorescence after lipase immobilization, which indirectly confirms the presence of enzyme biomolecules in the hybrid materials (Fig. 8). Microscopic images of MgO/Fuc and MgO/Fuc/LAN show a homogeneous structure in both modes (Fig. 8a). The images of ZrO<sub>2</sub>/Fuc (Fig. 8b) reveal small numbers of bright points, while the ZrO<sub>2</sub>/Fuc/LAN biocatalytic system emits more light.

In summary, the results obtained confirm that the functionalization of M<sub>x</sub>O<sub>y</sub> with fucoidan, and the subsequent immobilization of lipase, were successfully carried out. Based on the spectroscopic analysis a mechanism of interaction between the oxide materials, fucoidan and the enzyme was proposed (Fig. 9). As shown, fucoidan attaches directly to the MgO surface and hydrogen bonds are formed, while the hydrogen bonds between fucoidan and ZrO<sub>2</sub> are generated via water molecules. Between the support and the enzyme, only electrostatic interactions are present.

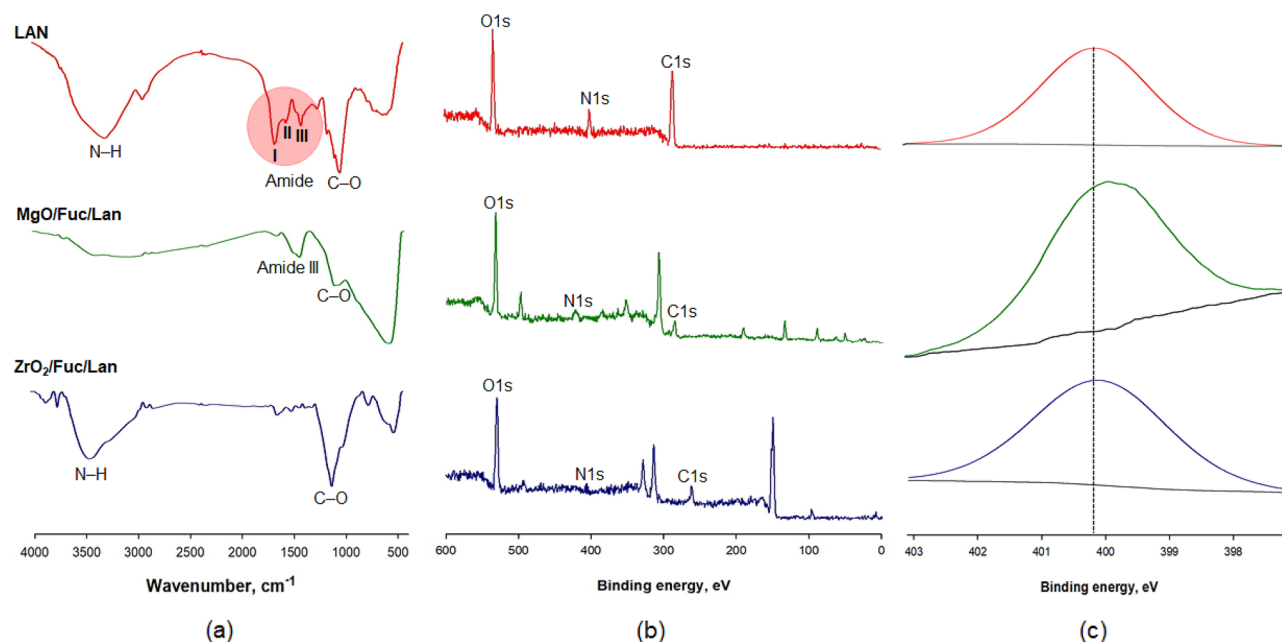


**Figure 7.** FTIR spectra of lipase, MgO/Fuc/LAN and ZrO<sub>2</sub>/Fuc/LAN (a). XPS survey spectra (b) and deconvolution of the N 1s line (c) for native lipase, MgO/Fuc/LAN and ZrO<sub>2</sub>/Fuc/LAN.

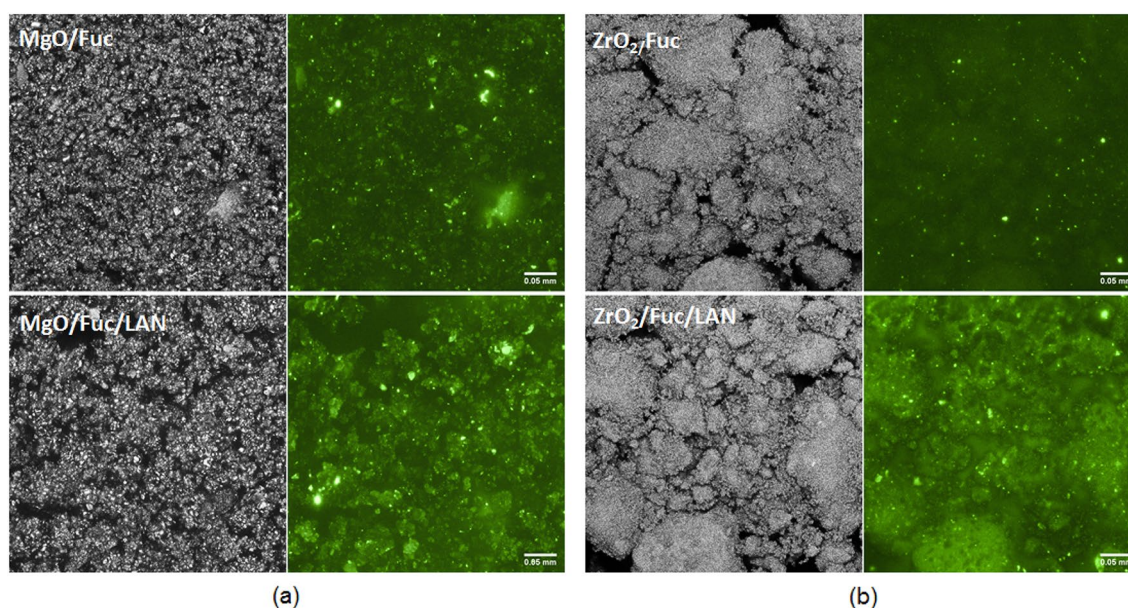


**Figure 8.** Confocal microscopy images of MgO/Fuc and MgO/Fuc/LAN (a); ZrO<sub>2</sub>/Fuc and ZrO<sub>2</sub>/Fuc/LAN (b) in reflection and fluorescence mode.

## Conclusion

In this study, new polysaccharide-based hybrids were fabricated and applied in lipase immobilization. The proposed hybrid materials were prepared by functionalizing magnesium (MgO) and zirconium (ZrO<sub>2</sub>) oxides with fucoidan from *Fucus vesiculosus*. Physicochemical analyses confirmed the effective modification of magnesium oxide and zirconia with fucoidan from *Fucus vesiculosus*. Tests of catalytic properties showed that the fabricated M<sub>x</sub>O<sub>y</sub>/hybrids can be used as supports for lipase from *Aspergillus niger* immobilization. Enhanced enzymatic activity (approximately 145 U/g) was achieved, and the obtained biocatalytic systems can be used over several enzymatic cycles, retaining a high percentage of their initial activity. The kinetic parameters show that the immobilized lipase can catalyze the enzymatic reaction faster than their free form. The results obtained in these experiments show that hybrids based on fucoidan and inorganic oxide can be successfully utilized in enzyme immobilization.

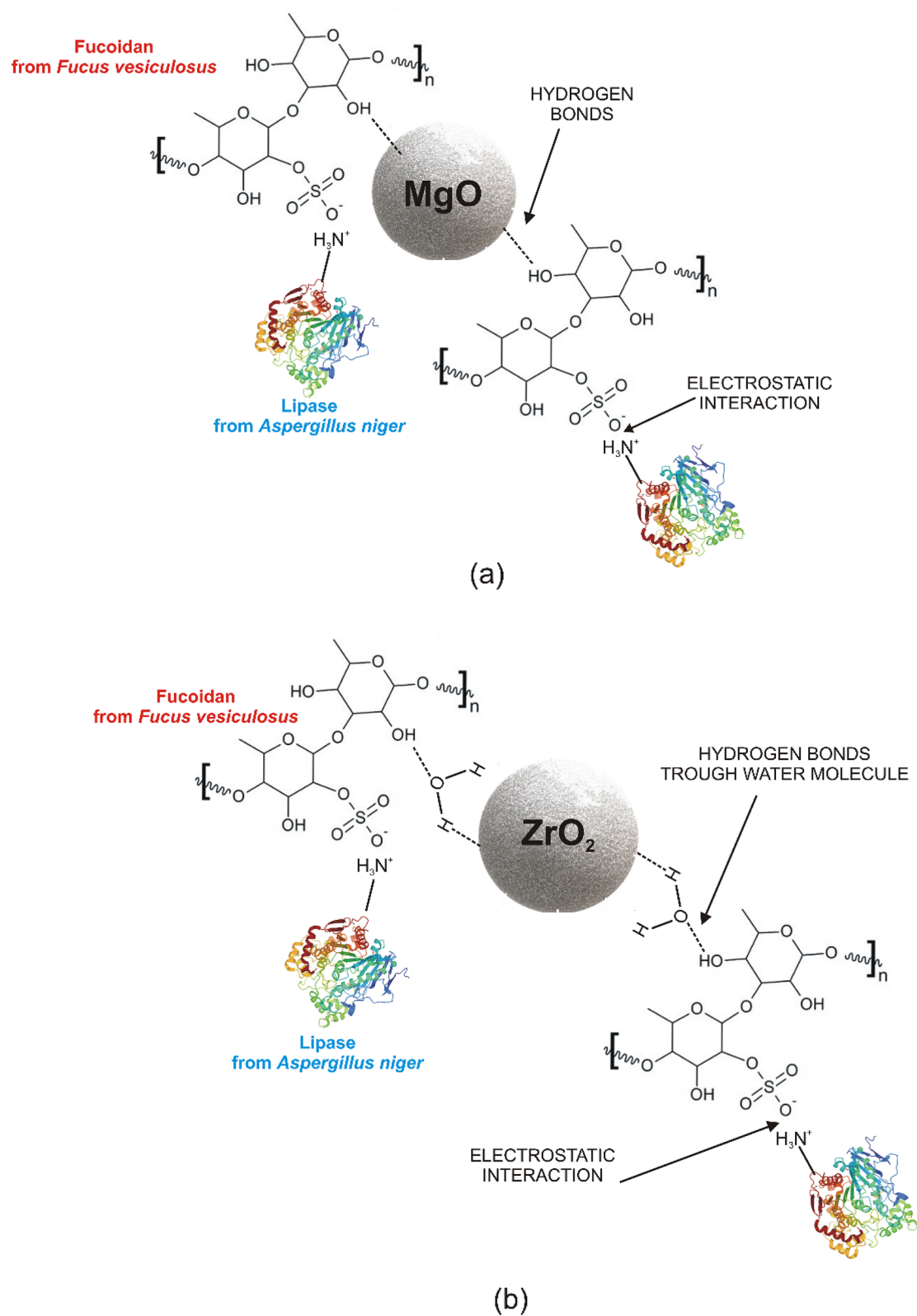


**Figure 9.** Proposed mechanism of interaction between the oxide support: MgO (a) and ZrO<sub>2</sub> (b), fucoidan, and lipase.

## Data availability

All data generated or analyzed during this study are included in this published article (and its Supplementary Information files).

Received: 21 February 2022; Accepted: 21 April 2022

Published online: 04 May 2022

## References

- Imam, A. *et al.* Application of laccase immobilized rice straw biochar for anthracene degradation. *Environ. Pollut.* **268**, 115827 (2021).
- de Souza Bezerra, T. M., Bassan, J. C., de Oliveira Santos, V. T., Ferraz, A. & Montib, R. Covalent immobilization of laccase in green coconut fiber and use in clarification of apple juice. *Process Biochem.* **50**, 417–423 (2015).
- Suman, S. K., Patnam, P. L., Ghosh, S. & Jain, S. L. Chicken feather derived novel support material for immobilization of laccase and its application in oxidation of veratryl alcohol. *ACS Sustain. Chem. Eng.* **7**, 3464–3474 (2019).
- Li, F.-L. *et al.* Specific immobilization of *Escherichia coli* expressing recombinant glycerol dehydrogenase on mannose-functionalized magnetic nanoparticles. *Catalysts* **9**, 7 (2019).
- Zhuang, M.-Y. *et al.* Using concanavalinA as a spacer for immobilization of *E. coli* on magnetic nanoparticles. *Int. J. Biol. Macromol.* **104**, 63–69 (2017).
- Bilal, M. & Iqbal, H. M. N. Naturally-derived biopolymers: Potential platforms for enzyme immobilization. *Int. J. Biol. Macromol.* **130**, 462–482 (2019).
- Sharma, A., Thatai, K. S., Kuthiala, T., Singh, G. & Arya, S. K. Employment of polysaccharides in enzyme immobilization. *React. Funct. Polym.* **167**, 105005 (2021).
- Zaitsev, S. Y., Savina, A. A. & Zaitsev, I. S. Biochemical aspects of lipase immobilization at polysaccharides for biotechnology. *Adv. Coll. Inter. Sci.* **272**, 102016 (2019).
- Shokri, Z. *et al.* Laccase immobilization onto natural polysaccharides for biosensing and biodegradation. *Carbohydr. Polym.* **262**, 117963 (2021).
- Wu, S. C., Wu, S. M. & Su, F. M. Novel process for immobilizing an enzyme on a bacterial cellulose membrane through repeated absorption. *J. Chem. Technol. Biotechnol.* **92**, 109–114 (2017).
- Je, H. H. *et al.* Cellulose nanofibers for magnetically separable and highly loaded enzyme immobilization. *Chem. Eng. J.* **323**, 425–433 (2017).
- Zdarta, J. *et al.* Chitin-lignin material as a novel matrix for enzyme immobilization. *Mar. Drugs* **13**, 2424–2446 (2015).
- Mei, S. *et al.* One-pot fabrication of chitin-shellac composite microspheres for efficient enzyme immobilization. *J. Biotechnol.* **266**, 1–8 (2018).
- Urrutia, P., Bernal, C., Wilson, L. & Illanes, A. Use of chitosan heterofunctionality for enzyme immobilization:  $\beta$ -galactosidase immobilization for galacto-oligosaccharide synthesis. *Int. J. Biol. Macromol.* **116**, 182–193 (2018).
- Facin, B. R., Moret, B., Baretta, D., Belfiore, L. A. & Paulino, A. T. Immobilization and controlled release of  $\beta$ -galactosidase from chitosan-grafted hydrogels. *Food Chem.* **179**, 44–51 (2015).
- de Oliveira, R. L., Dias, J. L., da Silva, O. S. & Porto, T. S. Immobilization of pectinase from *Aspergillus aculeatus* in alginate beads and clarification of apple and umbu juices in a packed bed reactor. *Food Bioprod. Process.* **109**, 9–18 (2018).
- Won, K., Kim, S., Kim, K.-J., Park, H. W. & Moon, S.-J. Optimization of lipase entrapment in Ca-alginate gel beads. *Process Biochem.* **40**, 2149–2154 (2005).
- Arana-Pena, S., Lokha, Y. & Fernandez-Lafuente, R. Immobilization of eversa lipase on octyl agarose beads and preliminary characterization of stability and activity features. *Catalysts* **8**, 511 (2018).
- Mateo, C. *et al.* Glyoxyl agarose: A fully inert and hydrophilic support for immobilization and high stabilization of proteins. *Enzym. Microb. Technol.* **39**, 274–280 (2006).
- Zucca, P., Fernandez-Lafuente, R. & Sanjust, E. Agarose and its derivatives as supports for enzyme immobilization. *Molecules* **21**, 1577 (2016).
- Hassan, M. E., Yang, Q. & Xiao, Z. Covalent immobilization of glucoamylase enzyme onto chemically activated surface of  $\kappa$ -carrageenan. *Bull. Natl. Res. Cent.* **43**, 102 (2019).
- Makas, Y. G., Kalkan, N. A., Aksoy, S., Altinok, H. & Hasirci, N. Immobilization of laccase in  $\kappa$ -carrageenan based semi-interpenetrating polymer networks. *J. Biotechnol.* **148**, 216–220 (2010).
- Huang, W. *et al.* Enzyme-catalyzed deposition of polydopamine for amplifying the signal inhibition to a novel Prussian blue-nanocomposite and ultrasensitive electrochemical immunosensing. *J. Mater. Sci. Technol.* **102**, 166–173 (2022).
- Xue, Y., Chen, J., Zhang, L. & Han, Y. BSA-lysozyme coated  $\text{NaCa}_2\text{HSi}_3\text{O}_9$  nanorods on titanium for cytocompatibility and antibacterial activity. *J. Mater. Sci. Technol.* **88**, 240–249 (2021).
- Ricardi, N. C. *et al.* Highly stable novel silica/chitosan support for  $\beta$ -galactosidase immobilization for application in dairy technology. *Food Chem.* **246**, 343–350 (2018).
- Alnadari, F. *et al.* Immobilization of  $\beta$ -glucosidase from *Thermatoga maritime* on chitin-functionalized magnetic nanoparticle via a novel thermostable chitin-binding domain. *Sci. Rep.* **10**, 1663 (2020).
- Drozd, R., Rakoczy, R., Wasak, A., Junka, A. & Fijałkowski, K. The application of magnetically modified bacterial cellulose for immobilization of laccase. *Int. J. Biol. Macromol.* **108**, 462–470 (2018).
- Zdarta, J. *et al.* Biopolymers conjugated with magnetite as support materials for trypsin immobilization and protein digestion. *Colloid Surf. B* **169**, 118–125 (2018).
- Fernando, I. P. S., Kim, D., Nah, J. W. & Jeon, Y. J. Advances in functionalizing fucoidans and alginates (bio)polymers by structural modifications: A review. *Chem. Eng. J.* **355**, 33–48 (2019).
- Zayed, A. & Ulber, R. Fucoidan production: Approval key challenges and opportunities. *Carbohydr. Polym.* **211**, 289–297 (2019).
- Balboa, E. M., Conde, E., Moure, A., Falqué, E. & Domínguez, H. In vitro antioxidant properties of crude extracts and compounds from brown algae. *Food Chem.* **138**, 1764–1785 (2013).
- Kim, K.-J., Lee, O.-H. & Lee, B.-Y. Fucoidan, a sulfated polysaccharide, inhibits adipogenesis through the mitogen-activated protein kinase pathway in 3T3-L1 preadipocytes. *Life Sci.* **86**, 791–797 (2010).
- Manivasagana, P. & Oha, J. Marine polysaccharide-based nanomaterials as a novel source of nanobiotechnological applications. *Int. J. Biol. Macromol.* **82**, 315–327 (2016).
- Tutor Ale, M. & Meyer, A. S. Fucoidans from brown seaweeds: An update on structures, extraction techniques and use of enzymes as tools for structural elucidation. *RSC Adv.* **3**, 8131 (2013).
- Moga, M. A. *et al.* Are bioactive molecules from seaweeds a novel and challenging option for the prevention of HPV infection and cervical cancer therapy?—A Review. *Int. J. Mol. Sci.* **22**, 629 (2021).
- Mansour, M. B. *et al.* Primary structure and anticoagulant activity of fucoidan from the sea cucumber *Holothuria polii*. *Int. J. Biol. Macromol.* **121**, 1145–1153 (2019).
- Zhao, Y. *et al.* Fucoidan extracted from *Undaria pinnatifida*: Source for nutraceuticals/functional foods. *Mar. Drugs* **16**, 321 (2018).

38. Luthuli, S. *et al.* Therapeutic effects of fucoidan: A review on recent studies. *Mar. Drugs* **17**, 487 (2019).
39. Pajovich, H. T. & Banerjee, I. A. Biom mineralization of fucoidan-peptide blends and their potential applications in bone tissue regeneration. *J. Funct. Biomater.* **8**, 41 (2017).
40. Tutor Ale, M., Mikkelsen, J. D. & Meyer, A. S. Important determinants for fucoidan bioactivity: A critical review of structure-function relations and extraction methods for fucose-containing sulfated polysaccharides from brown seaweeds. *Mar. Drugs* **9**, 2106–2130 (2011).
41. van Weelden, G. *et al.* Fucoidan structure and activity in relation to anti-cancer mechanisms. *Mar. Drugs* **17**, 32–62 (2019).
42. Li, B., Lu, F., Wei, X. & Zhao, R. Fucoidan: Structure and bioactivity. *Molecules* **13**, 1671–1695 (2008).
43. Lorbeer, A. J. *et al.* Sequential extraction and characterization of fucoidans and alginates from *Ecklonia radiata*, *Macrocystis pyrifera*, *Durvillaea potatorum*, and *Seirococcus axillaris*. *J. Appl. Phycol.* **29**, 1515–1526 (2017).
44. Lahrssen, E., Liewert, I. & Alban, S. Gradual degradation of fucoidan from *Fucus vesiculosus* and its effect on structure, antioxidant and antiproliferative activities. *Carbohydr. Polym.* **192**, 208–216 (2018).
45. Chiang, C.-S. *et al.* Fucoidan-based nanoparticles with inherently therapeutic efficacy for cancer treatment. *Pharmaceutics* **13**, 1986 (2021).
46. Venkatesan, J., Bhatnagar, I. & Kim, S.-K. Chitosan-alginate biocomposite containing fucoidan for bone tissue engineering. *Mar. Drugs* **12**, 300–316 (2014).
47. Changotade, S. *et al.* Potential effects of a low-molecular-weight fucoidan extracted from brown algae on bone biomaterial osteoconductive properties. *J. Biomed. Mater. Res. A* **87**, 666–675 (2008).
48. Moorthy, M. S. *et al.* Fucoidan-coated core-shell magnetic mesoporous silica nanoparticles for chemotherapy and magnetic hyperthermia-based thermal therapy applications. *New J. Chem.* **41**, 15334 (2017).
49. Jang, B. *et al.* Fucoidan-coated CuS nanoparticles for chemo- and photothermal therapy against cancer. *Oncotarget* **9**, 12649–12661 (2018).
50. Shin, S.-W. *et al.* Fucoidan-manganese dioxide nanoparticles potentiate radiation therapy by co-targeting tumor hypoxia and angiogenesis. *Mar. Drugs* **16**, 510 (2018).
51. Venkatesan, J., Singh, S. K., Anil, S., Kim, S.-K. & Shim, M. S. Preparation, characterization and biological applications of biosynthesized silver nanoparticles with chitosan-fucoidan coating. *Molecules* **23**, 1429 (2018).
52. Nguyen, H. *et al.* Bimodal fucoidan-coated zinc oxide/iron oxide-based nanoparticles for the imaging of atherothrombosis. *Molecules* **24**, 962 (2019).
53. Bradford, M. M. A rapid and sensitive method for the quantitation of microgram quantities of protein utilizing the principle of protein-dye binding. *Anal. Biochem.* **72**, 248–254 (1976).
54. Sinurat, E., Saepudin, E., Peranginangin, R. & Hudiyono, S. Immunostimulatory activity of brown seaweed-derived fucoidans at different molecular weights and purity levels towards white spot syndrome virus (WSSV) in shrimp *Litopenaeus vannamei*. *J. Appl. Pharm. Sci.* **6**, 082–091 (2016).
55. Zayed, A. *et al.* Physicochemical and biological characterization of fucoidan from *Fucus vesiculosus* purified by dye affinity chromatography. *Mar. Drugs* **14**, 79 (2016).
56. Vilela, C. *et al.* Conductive polysaccharides-based proton-exchange membranes for fuel cell applications: The case of bacterial cellulose and fucoidan. *Carbohydr. Polym.* **230**, 115604 (2019).
57. Lai, Y.-H., Chiang, C.-S., Hsu, C.-H., Cheng, H.-W. & Chen, S.-Y. Development and characterization of a fucoidan-based drug delivery system by using hydrophilic anticancer polysaccharides to simultaneously deliver hydrophobic anticancer drugs. *Biomolecules* **10**, 970 (2020).
58. Lim, S. J. *et al.* Characterization of fucoidan extracted from *Malaysian Sargassum binderi*. *Food Chem.* **209**, 267–273 (2016).
59. Xie, W. & Huang, M. Enzymatic production of biodiesel using immobilized lipase on core-shell structured Fe<sub>3</sub>O<sub>4</sub>@MIL-100(Fe) composites. *Catalysts* **9**, 850 (2019).
60. Chen, M. *et al.* Synthesis of chitin/graphene oxide composite aerogel beads for lipase immobilization. *J. Porous Mater.* **27**, 549–554 (2020).
61. Xiang, X. *et al.* Fabrication of chitosan-mesoporous silica SBA-15 nanocomposites via functional ionic liquid as the bridging agent for PPL immobilization. *Carbohydr. Polym.* **182**, 245–253 (2018).
62. Osuna, Y. *et al.* Immobilization of *Aspergillus niger* lipase on chitosan-coated magnetic nanoparticles using two covalent-binding methods. *Bioprocess Biosyst. Eng.* **38**, 1437–1445 (2015).
63. Park, S., Oh, Y., Jung, D. & Lee, S. H. Effect of cellulose solvents on the characteristics of cellulose/Fe<sub>2</sub>O<sub>3</sub> hydrogel microspheres as enzyme supports. *Polymers* **12**, 1869 (2020).

## Author contributions

Conceptualization; Data curation; formal analysis; methodology; roles/writing—original draft—A.K.-R.; Formal analysis; writing—review and editing—M.B.; Formal analysis—A.B., supervision; writing—review and editing—T.J. All authors have read and agreed to the published version of the manuscript.

## Funding

This research was funded by the National Science Center Poland, under the program MINIATURA 4, grant number: 2020/04/X/ST5/00318.

## Competing interests

The authors declare no competing interests.

## Additional information

**Supplementary Information** The online version contains supplementary material available at <https://doi.org/10.1038/s41598-022-11319-0>.

**Correspondence** and requests for materials should be addressed to A.K.-R.

**Reprints and permissions information** is available at [www.nature.com/reprints](http://www.nature.com/reprints).

**Publisher's note** Springer Nature remains neutral with regard to jurisdictional claims in published maps and institutional affiliations.



**Open Access** This article is licensed under a Creative Commons Attribution 4.0 International License, which permits use, sharing, adaptation, distribution and reproduction in any medium or format, as long as you give appropriate credit to the original author(s) and the source, provide a link to the Creative Commons licence, and indicate if changes were made. The images or other third party material in this article are included in the article's Creative Commons licence, unless indicated otherwise in a credit line to the material. If material is not included in the article's Creative Commons licence and your intended use is not permitted by statutory regulation or exceeds the permitted use, you will need to obtain permission directly from the copyright holder. To view a copy of this licence, visit <http://creativecommons.org/licenses/by/4.0/>.

© The Author(s) 2022